Partitioned Coupling for Structural Acoustics

Gregory Bunting
Computational Solid Mechanics and Structural Dynamics,
Sandia National Laboratories,
P.O. Box 5800,
Albuquerque, NM 87185-0845
e-mail: gbuntin@sandia.gov

Scott T. Miller
Computational Solid Mechanics and Structural Dynamics,
Sandia National Laboratories,
P.O. Box 5800,
Albuquerque, NM 87185-0845
e-mail: stmille@sandia.gov

*We expand the second-order fluid–structure coupling scheme of Farhat et al. (1998, "Load and Motion Transfer Algorithms for 19 Fluid/Structure Interaction Problems With Non-Matching Discrete Interfaces: Momentum and Energy Conservation, Optimal Discretization and Application to Aeroelasticity," Comput. Methods Appl. Mech. Eng., **157**(1–2), pp. 95–114; 2006, "Provably Second-Order Time-Accurate Loosely-Coupled Solution Algorithms for Transient Nonlinear Computational Aeroelasticity," Comput. Methods Appl. Mech. Eng., **195**(17), pp. 1973–2001) to structural acoustics. The staggered structural acoustics solution method is demonstrated to be second-order accurate in time, and numerical results are compared to a monolithically coupled system. The partitioned coupling method is implemented in the Sierra Mechanics software suite, allowing for the loose coupling of time domain acoustics in SIERRA/SD to structural dynamics (SIERRA/SD) or solid mechanics (SIERRA/SM). The coupling is demonstrated to work for nonconforming meshes. Results are verified for a one-dimensional piston, and the staggered and monolithic results are compared to an exact solution. Huang, H. (1969, "Transient Interaction of Plane Acoustic Waves With a Spherical Elastic Shell," J. Acoust. Soc. Am., **45**(3), pp. 661–670) sphere scattering problem with a spherically spreading acoustic load demonstrates parallel capability on a complex problem. Our numerical results compare well for a bronze plate submerged in water and sinusoidally excited (Fahnline and Shepherd, 2017, "Transient Finite Element/Equivalent Sources Using Direct Coupling and Treating the Acoustic Coupling Matrix as Sparse," J. Acoust. Soc. Am., **142**(2), pp. 1011–1024).*
[DOI: 10.1115/1.4045215]

Keywords: aeroelasticity, dynamics, structural acoustics

1 Introduction

Structural acoustics involves the interaction between a vibrating structure and the pressure fluctuations in an acoustic field, and it can be useful in identifying the noise radiated from a structure or how a structure responds to acoustic waves. Applications of coupled structural acoustics include shock loads on ships [1,2], tire–road interaction [3–5], and aero-structures [6–9]. Computational structural acoustics is used at Sandia National Laboratories to predict structural responses in various acoustic environments. Figure 1 shows a weapons system in an acoustic loading environment. There are also a multitude of well-studied academic problems, including plates, spheres, cylinders, and other basic structures suspended in acoustic media [10–12]. Many applications include unbounded domains where special treatments are required to solve a finite sized problem: Infinite elements [13] and perfectly matched layers [14] are two possible ways to calculate the acoustic response in a unbounded or non-reflecting region of interest.

Various computational schemes can be used to calculate structural acoustic responses [15]. Typically, finite elements are used for the structural domain, and either finite elements or boundary elements are used for the acoustic domain [12]. Structural acoustics problems can be solved in the time domain, the frequency domain, or with modal superposition which requires solving a quadratic eigenvalue problem. This work focuses on the solution of the structural acoustic problem in the time domain.

When the behavior of the fluid is minimally affected by the structure, the fluid problem can be solved a priori, and the solution to the fluid problem can be used to load the structure in a one-way coupling scheme. Complex fluid–structure interactions necessitate two-way coupling, where the fluid and the structure mutually influence each other and must march forward in time together. For two-way coupling, the governing equations can be solved in a monolithic approach or a loosely coupled approach [16,17]. Structural acoustic implementations using monolithic coupling methods solve the discretized governing equations with all the degrees-of-freedom in both the structural and acoustic models [15,18,19]. These fully coupled methods provide second-order accuracy, are well studied, and are simple to implement. However, fully coupled systems can induce poorly conditioned linear systems due to vast differences in the material properties between a solid such as steel and a fluid such as air. While a direct linear algebra solver can handle these differences, parallel iterative solvers struggle (relative residual order of magnitude). Many parallel solvers are optimized for symmetric dynamic matrices; however, the coupling terms between the two domains break the symmetry of the system. Issues of solve time and solver convergence become significant obstacles when solving large, massively parallel, real-world structural acoustic software. An alternative to solving the fully coupled system is to use an iterative loose-coupling approach.

While loosely coupled time integration implementations are relatively uncommon in structural acoustics applications [18–22], they are common in fluid–structure problems that solve the full Navier–Stokes system of equations [16,23]. This is often because fluid applications and structural applications are developed independently and then coupled in an multiple program-multiple data (MPMD) method that prohibits solving the governing equations monolithically. Historically, second-order accuracy has been achieved in these applications using iterative methods at each time step of the coupled system. Farhat et al. have developed the generalized serial staggered coupling algorithm and show that it is second-order accurate in time [16,17]. Rather than iterating to solution convergence, the loosely coupled fluid–structure interaction problem is solved with exactly one prediction and one

Contributed by the Noise Control and Acoustics Division of ASME for publication in the JOURNAL OF VIBRATION AND ACOUSTICS. Manuscript received May 6, 2019; final manuscript received October 3, 2019; published online October 16, 2019. Assoc. Editor: Julian Rimoli.

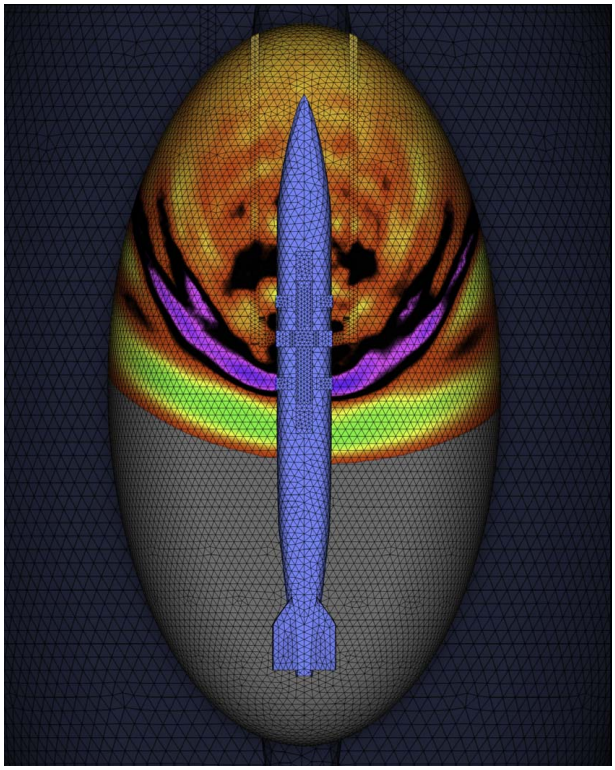

Fig. 1 Weapons system in an acoustic loading environment

correction step. In this work, the general serialized staggered (GSS) algorithm is extended to present a loose structure–acoustic coupling algorithm that is second-order accurate in time. This decouples the structural and acoustic equations and alleviates the scaling and condition problems associated with the strongly coupled problem. Other advantages of this method include optimization of solver parameters on each subdomain and faster computation time, while maintaining the accuracy of the strongly coupled solution.

An added benefit of this approach is that in massively parallel applications with legacy software, this approach can be used to couple separate finite element programs without needing to mix source code. Furthermore, the flexibility offered by loosely coupling allows both the fluid and the structure codes to be interchanged depending on the needs of the particular application.

The monolithic coupling was implemented in the massively parallel structural dynamics finite element code SIERRA/SD [24–27]. The loosely coupled algorithm was implemented first by launching two instances of SIERRA/SD and communicating through an MPI-based MPMD coupler [28]. The coupler necessitated communication only on the structural-acoustic interface. That is, processors that contained only structural elements and no interface with acoustic elements needed no MPI communication, and vice versa. Processors that contained the structural acoustic interface need only to communicate the nodal locations on the interface, as well as the pressures, velocities, and accelerations at those nodal locations.

In addition to the coupling method discussed above, there are a number of application specific algorithmic decisions that are made when solving a structural acoustic problem. These include the choice of finite elements versus boundary elements for the acoustic domain, and conforming of mis-matched meshes at the domain boundary, and one-way or two-way coupling. While not the primary subject of this work, some context is provided to show the decisions made in this implementation. As such, it is understood that boundary elements, conforming meshes, and one-way coupling are all valid algorithmic approaches that are not the focus of this work.

One-way coupling can be used in an application such as aero-structure analysis, where a fluid flow is used to load a structure, and the displacements, accelerations, or stresses of the structure are the quantity of interest, and it is assumed that the movement of the structure has minimal effect on the fluid flow. However, if the quantity of interest is in the fluid domain, and the movement of the structure is expected to have an effect on that quantity, two-way coupling is necessary to capture that behavior.

Having the same mesh density in the acoustic fluid and solid may be very inefficient, since the two domains typically require significantly different mesh densities to achieve a given level of discretization accuracy. Perhaps, more importantly, it is also impractical in many applications since the mesh generation process may be performed separately for the two domains. Generating conforming meshes on the wet interface may be very difficult, if not impossible, even given the most sophisticated mesh generation software. Illustrative examples include the hull of a ship [29] or the skin of an aircraft. In these cases, the structural and fluid meshes are typically created independently and have very different mesh density requirements. Joining them into a single, monolithic mesh is often impractical. The node-on-face structural acoustic coupling method is used. For a detailed description of the procedure, see Ref. [17].

2 Theory

2.1 Governing Equations. We consider a simply connected three-dimensional domain Ω that consists of disjoint subsets Ω_s and Ω_a such that $\Omega = \Omega_s \cup \Omega_a$ and $\Omega_s \cap \Omega_a = \emptyset$. We refer to Ω_s as the structural domain and Ω_a as the acoustic domain. The boundary of each of these domains is divided into disjoint Dirichlet, Neumann, and structure–acoustic coupling partitions. As such, $\partial\Omega_k = \Gamma_k^D \cup \Gamma_k^N \cup \Gamma_{sa}$ for $k = \{s, a\}$. The boundary of the complete domain of interest is the union of the Dirichlet and Neumann components of each subdomain.

2.1.1 Structural Dynamics. The equation of motion for (possibly damped) structural dynamics is the standard linearized elastodynamics equation

$$\rho_s \ddot{\mathbf{u}} + \mathbf{C}_s \dot{\mathbf{u}} - \nabla \cdot \mathbf{T}_R = \rho_s \mathbf{b} \tag{1}$$

where ρ_s is the mass density, $\mathbf{u}$ is the displacement field, $\mathbf{C}_s$ is the damping coefficient, $\mathbf{T}_R$ is the first Piola–Kirchhoff stress tensor, and $\mathbf{b}$ is a mass-specific body force. The subscript "s" is used to denote a structural quantity when the same symbol is used for an acoustic quantity. The constitutive equation is

$$\mathbf{T}_R = \mathbb{C}[\mathrm{Sym}(\nabla \mathbf{u})] = \lambda \,\mathrm{tr}(\nabla \mathbf{u})\mathbf{I} + 2\mu(\nabla \mathbf{u} + (\nabla \mathbf{u})^T) \tag{2}$$

where $\mathbb{C}$ is the elasticity tensor and λ and μ are the Lamé parameters. Initial conditions are

$$\mathbf{u}(\mathbf{X}, t = t_0) = \mathbf{u}_0 \quad \forall \mathbf{X} \in \Omega_s \tag{3a}$$

$$\dot{\mathbf{u}}(\mathbf{X}, t = t_0) = \dot{\mathbf{u}}_0 \quad \forall \mathbf{X} \in \Omega_s \tag{3b}$$

Dirichlet and Neumann boundary conditions are specified as

$$\mathbf{u} = \mathbf{g}_s \quad \text{on } \Gamma_s^D \tag{4a}$$

$$\mathbf{T}_R[\mathbf{n}] = \mathbf{t}_s = \mathbf{h}_s \quad \text{on } \Gamma_s^N \tag{4b}$$

where $\mathbf{n}$ is the outward normal vector on the boundary and $\mathbf{t}_s$ is the traction.

2.1.2 Acoustics. The linearized Euler equations are combined into a single equation for velocity potential as

$$\frac{1}{c_a^2}\ddot{\psi} + C_a\dot{\psi} - \nabla^2\psi = 0 \tag{5}$$

where ψ is the velocity potential such that $\mathbf{v}_a = \nabla\psi$, and the acoustic wavespeed is c_a. The damping coefficient is C_a. The subscript "a" is

used to denote an acoustic quantity when the same symbol is used for a structural quantity. The acoustic pressure is obtained via $p = \dot{\psi}$, which is slightly different from the typical velocity potential equation for linearized acoustics. This choice was made based on linear solver considerations of our monolithic coupling formulation, described in Sec. 2.4. Initial and boundary conditions are given as

$$\psi(\mathbf{X}, t = t_0) = \psi_0 \quad \forall \mathbf{X} \in \Omega_a \tag{6a}$$

$$\dot{\psi}(\mathbf{X}, t = t_0) = \dot{\psi}_0 \quad \forall \mathbf{X} \in \Omega_a \tag{6b}$$

$$\psi = \mathbf{g}_a \quad \text{on } \Gamma_a^D \tag{6c}$$

$$\nabla\psi \cdot \mathbf{n} = h_a \quad \text{on } \Gamma_a^N \tag{6d}$$

2.1.3 Coupling Conditions. The structure and the acoustic are coupled (in the strong sense) through velocity (**v**) and traction (**t**) continuity:

$$\mathbf{v}_s = \mathbf{v}_a = \nabla\psi \quad \text{on } \Gamma_{sa} \tag{7a}$$

$$\mathbf{t}_s = \mathbf{t}_a = -p\mathbf{n} \quad \text{on } \Gamma_{sa} \tag{7b}$$

where Γ_{sa} is the structure–acoustic boundary.

2.2 Semi-Discrete Form. The standard Galerkin finite element method is used to discretize (1) and (5) in space. The resulting semi-discrete system is given as

$$\begin{bmatrix} M_s & 0 \\ 0 & M_a \end{bmatrix}\begin{bmatrix} \ddot{\mathbf{u}} \\ \ddot{\psi} \end{bmatrix} + \begin{bmatrix} C_s & C_{sa} \\ C_{as} & C_a \end{bmatrix}\begin{bmatrix} \dot{\mathbf{u}} \\ \dot{\psi} \end{bmatrix} + \begin{bmatrix} K_s & 0 \\ 0 & K_a \end{bmatrix}\begin{bmatrix} \mathbf{u} \\ \psi \end{bmatrix} = \begin{bmatrix} \mathbf{f}_s \\ f_a \end{bmatrix} \tag{8}$$

where M, C, and K are mass, damping, and stiffness matrices. The matrices C_{sa} and C_{as} enforce the coupling conditions on the interface; expressions for the other sub-matrices of the system can be found in finite element textbooks, e.g., Refs. [30,31]. The structure–acoustic coupling matrix is determined by integrating the stress term of (1) by parts, and substituting (7*b*) on the resulting term defined over the structure–acoustic boundary. Similarly, the acoustic–structure matrix is defined when (5) is integrated by parts and (7*a*) is enforced on Γ_{sa}.

2.3 Time Integration. Newmark beta time integration

$$\theta^{n+1} = \theta^n + (\Delta t)\dot{\theta}^n + \frac{(\Delta t)^2}{2}\left\{(1-2\beta)\ddot{U}^n + 2\beta\ddot{U}^{n+1}\right\} \tag{9a}$$

$$\dot{\theta}^{n+1} = \dot{\theta}^n + (\Delta t)\left\{(1-\gamma)\ddot{\theta}^n + \gamma\ddot{\theta}^{n+1}\right\} \tag{9b}$$

is used to advance the solution from time t^n to t^{n+1} with a constant time step size Δt. θ is used to denote either **u** or ψ. The implicit, second-order time accurate and unconditionally stable version of the scheme is used, which requires $\beta = 1/4$ and $\gamma = 1/2$. The system in (8) is solved for displacement rather than acceleration.

2.4 Monolithic Coupling. Monolithic coupling of the structural and acoustic response is achieved by solving (8) combined with (9) as a single algebraic system for each time step. This results in a tightly coupled structural–acoustic response and is second-order accurate in time. Matrix ill-conditioning can occur when the densities of the acoustic and structural materials are severely disparate.

2.5 Interfield-Parallel Strategies. Interfield-parallel [32] strategies solve the acoustic and structural equations simultaneously. This requires predictions of both the structure velocity and acoustic pressure. One simple predictor is

$$\dot{\mathbf{u}}_s^P = \dot{\mathbf{u}}_s(t^n) \tag{10}$$

$$p_a^P = p_a(t^n) \tag{11}$$

which results in first-order accuracy. Loose coupling with interfield-parallel solutions results in first-order accuracy: the loading is never corrected with updated solution data. As such, results are presented using serial solution strategies.

2.6 Serial Solution Strategies. Serial solution strategies solve the acoustic and structural equations sequentially. This requires predictions of either structure acceleration or acoustic pressure. The load on the second solve is corrected with information from the first solve. Numerous combinations of predictors/correctors have been proposed for the fluid–structure interaction. However, there is a gap in the literature for loosely coupled structural acoustics. The predictions currently available in the structural-acoustic literature result in first-order accuracy.

The GSS procedure from Ref. [16] was designed as a coupling algorithm to preserve accuracy of the time integrator for moving meshes. Figure 2 shows the logic flowchart for the GSS algorithm.

Even though our meshes are not moving, we have found the GSS algorithm essential for maintaining time accuracy.

To solve (8) in a partitioned manner, we apply a predictor–corrector algorithm as in Ref. [16]. We apply the second-order accurate (Adams–Bashforth) predictor for the structural velocities as suggested in Refs. [16,23]

$$\dot{\mathbf{u}}^{n+1^P} = \dot{\mathbf{u}}^n + \frac{3}{2}\Delta t\ddot{\mathbf{u}}^n - \frac{1}{2}\Delta t\ddot{\mathbf{u}}^{n-1} \tag{12}$$

The corrected pressure is taken to be the end-of-step value, i.e.,

$$p^{n+1^C} = \dot{\psi}^{n+1^C} = \psi^{n+1} \tag{13}$$

With the predictor (12) and corrector (13), (8) is rewritten as

$$\begin{bmatrix} M_s & 0 \\ 0 & M_a \end{bmatrix}\begin{bmatrix} \ddot{\mathbf{u}} \\ \ddot{\psi} \end{bmatrix} + \begin{bmatrix} C_s & C_{sa} \\ 0 & C_a \end{bmatrix}\begin{bmatrix} \dot{\mathbf{u}} \\ \dot{\psi} \end{bmatrix} + \begin{bmatrix} K_s & 0 \\ 0 & K_a \end{bmatrix}\begin{bmatrix} \mathbf{u} \\ \psi \end{bmatrix} = \begin{bmatrix} \mathbf{f}_s \\ f_a \end{bmatrix} - \begin{bmatrix} 0 \\ C_{as}\dot{\mathbf{u}}^{n+1^P} \end{bmatrix} \tag{14}$$

Equation (14) can now be solved for ψ independently of **u**; hence, it is a partitioned algorithm. Since the predictor (12) and the Newmark beta time integrator (9) are second-order time accurate, the resulting partitioned algorithm is second-order accurate in time. Numerical results in Sec. 3.1 demonstrate the temporal accuracy of the method.

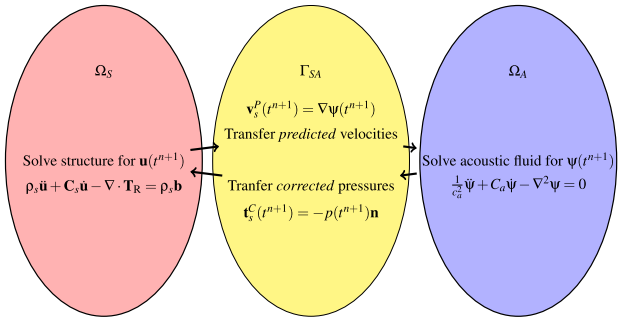

Fig. 2 GSS algorithm

3 Numerical Examples

3.1 Verification in One Dimension: A Piston Example. Figure 3 illustrates a one-dimensional piston in an acoustic fluid. The verification problem consists of exactly one degree-of-freedom on the structural mesh and exactly one degree-of-freedom on the acoustic mesh. It can also be produced by using a three-dimensional stiff plate on the structural mesh, and hex elements on the acoustics mesh. The exact solution for this problem is specified as

$$u(t) = e^{-dt}(a\cos\omega t + b\sin\omega t) + v(t-\beta) \tag{15}$$

$$v_a(t) = \dot{u}_s\left(t - \frac{x}{c_a}\right)H\left(t - \frac{x}{c_a}\right) \tag{16}$$

$$p_a(t) = p_\infty + \rho_a c_a v_a(t) \tag{17}$$

Figure 4 shows the convergence plot for the strong coupling solution. As expected and discussed in the literature, strong coupling gives second-order convergence with time.

Figure 5 shows the convergence plot for the loosely coupled solution. Following the GSS algorithm, we are able to show that the convergence plot for the loosely coupled system is also second-order accurate in time.

3.2 Huang Sphere. The Huang sphere [10] example is the response of an elastic shell sphere in an acoustic fluid. Figure 6 shows the sample problem of an elastic shell sphere in an acoustic medium. The shell is made up of a homogenous isotropic elastic material. Elastic motion of the shell is initiated by a incident shock wave, which is scattered by the shell. To see the specific details of the SIERRA/SD spherically spreading wave, see the users manual [24]. The acoustic medium is meshed with 1,340,623 tetrahedral (TET4) elements, and the elastic shell is meshed with 1944 four-noded shell elements (NQUAD). Furthermore, the acoustic

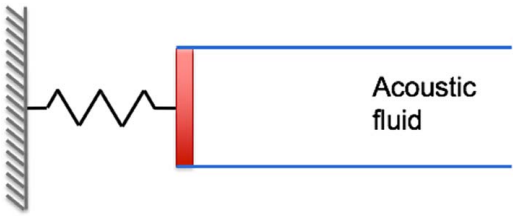

Fig. 3 1D structure attached to a semi-infinite acoustic fluid. Motion is constrained to move in the horizontal direction only.

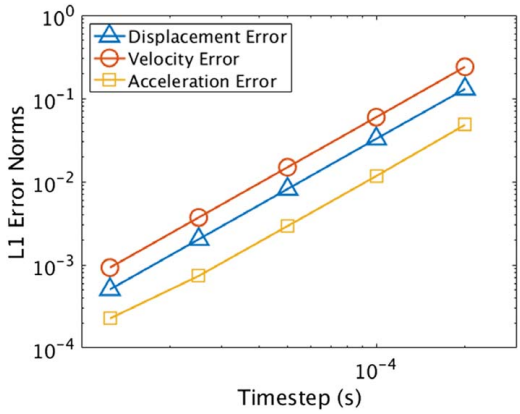

Fig. 4 Convergence plot for 1D piston—tightly coupled

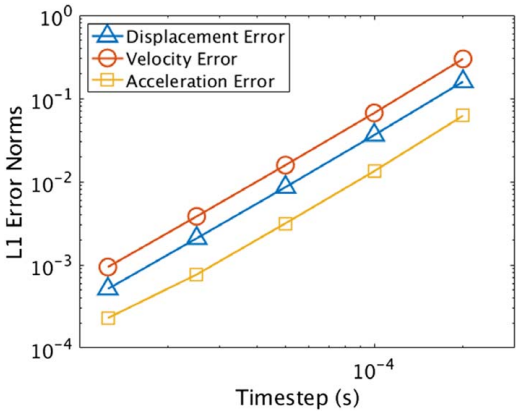

Fig. 5 Convergence plot for 1D piston—loosely coupled

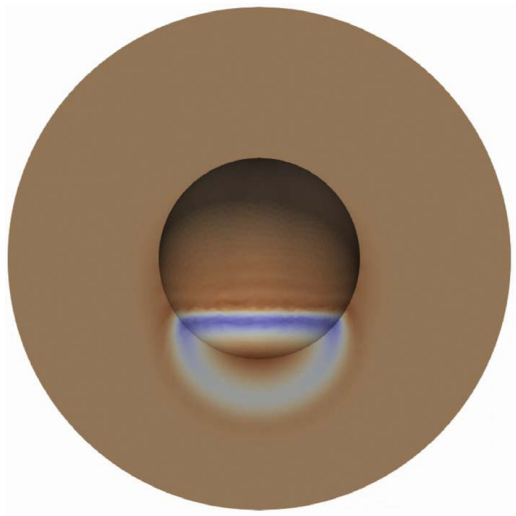

Fig. 6 Huang sphere—elastic shell in an acoustic medium (t = 1e − 4)

medium is surrounded by 31,940 eight-order infinite elements based on the Astley–Leis formulation using Legendre polynomial basis functions [13]. The problem is solved with a time step Δt = 1e − 6 for 2000 time steps. The spherically spreading load is applied at an origin of (0, 0, −30) and a reference location of (0, 0, −10). The load spreads outward along the acoustic–structure boundary with time. Figure 7 shows the velocity in the X direction at a node on the sphere with coordinates (10, 0, 0). Figure 8 shows the velocity in the Y direction at a node on the sphere with coordinates (0, −10, 0). These figures show that the loosely coupled approach matches the tightly coupled simulation.

3.3 Bronze Plate Example. The bronze plate example is detailed in Ref. [11]. It consists of a solid bronze plate submerged in water, with a drive point near one corner and an accelerometer in the middle of the same edge. The setup is depicted in Fig. 9.

The plate is 0.3048 m by 0.762 m by 0.04445 m. Density of bronze is 7468 kg/m^3. Young's modulus and Poisson's ratio are 117 GPa and 0.3, respectively. The force applied at the drive point is

$$f(t) = \begin{cases} 500\sin^2(\pi t/t_0)N & \text{for } t < t_0 \\ 0 & \text{otherwise} \end{cases} \tag{18}$$

where t_0 = 5.5e − 4 s. The plate is meshed with 1920 linear hexahedral elements.

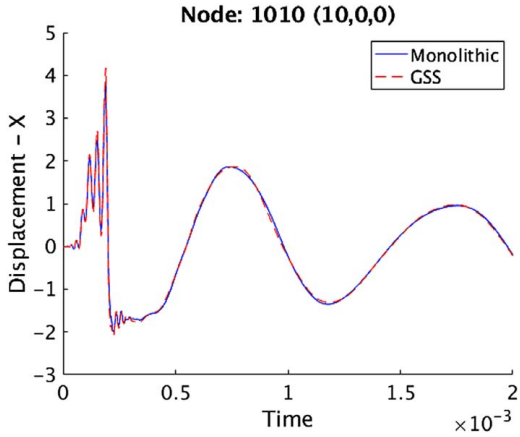

Fig. 7 *X*-velocity at node 1010

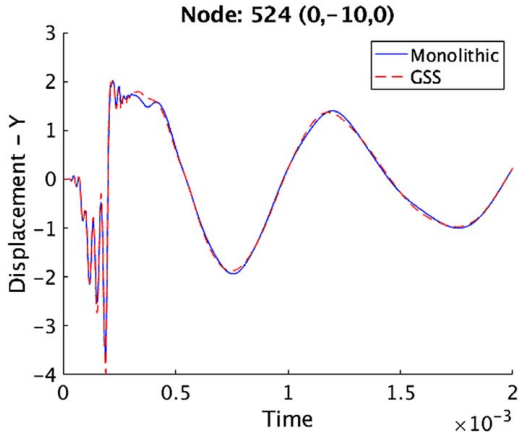

Fig. 8 *Y*-velocity at node 524

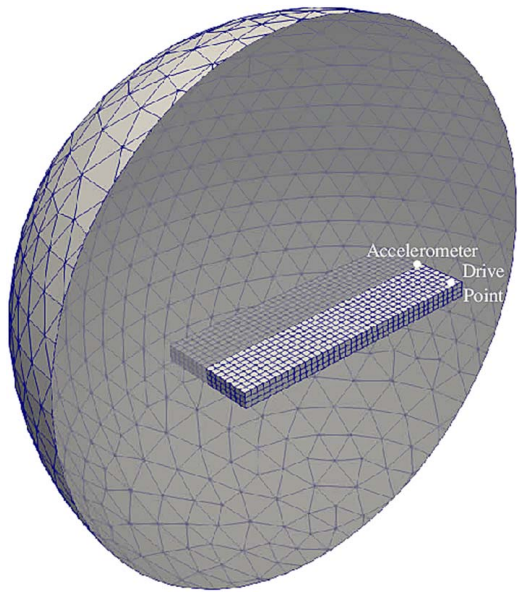

Fig. 9 Bronze plate meshed with hexahedra immersed in a tetrahedral acoustic region. Drive point and accelerometer locations are marked.

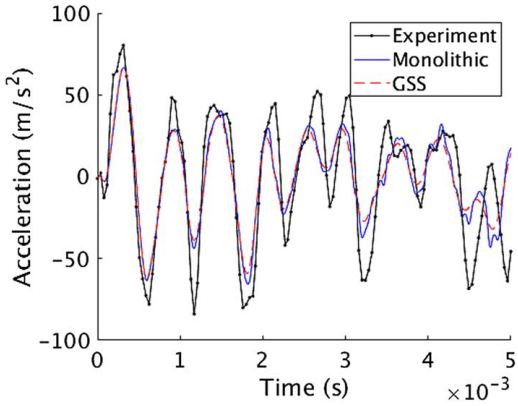

Fig. 10 Transverse acceleration at the accelerometer on the bronze plate

The plate is immersed in an acoustic fluid of radius $r = 1.6$ m. The acoustic mesh is composed of 188,664 linear tetrahedral elements. Tenth-order infinite elements are used on the outer boundary of the acoustic domain. Density of the water is 1000 kg/m^3. Acoustic sound speed is $c_0 = 1500$ m/s.

Figure 10 shows the GSS and monolithic numerical schemes compared to the experimental results from Ref. [11].

Both numerical schemes under-predict the amplitude of the experiment, but the period is captured well. The GSS scheme is seen to attenuate the structural vibrations faster than the monolithic solution.

4 Conclusions

A partitioned-coupling approach for structural acoustics based on the GSS algorithm was proposed. This method utilizes separate solves for the acoustic and structural domains, making it amenable to use with legacy software packages. Partitioning the system removes ill-conditioning concerns that arise in more traditional structural-acoustics solvers, where differences in material properties cause numerical problems for monolithic solution methods.

We demonstrated second-order time accuracy of the partitioned method on a quasi-one-dimensional piston problem. The Huang sphere and bronze plate examples show that the GSS approach yields solutions that are comparable to the monolithic solve for the same problem. Additionally, the bronze plate results match experimental data within reasonable tolerances.

Acknowledgment

Sandia National Laboratories is a multimission laboratory managed and operated by National Technology and Engineering Solutions of Sandia, LLC, a wholly owned subsidiary of Honeywell International Inc. for the U.S. Department of Energy's National Nuclear Security Administration under contract DE-NA0003525 (Funder ID: 10.13039/100000015).

The SIERRA/SD software package is the collective effort of many individuals and teams. The core Sandia National Laboratories-based SIERRA/SD development team responsible for the maintenance of documentation and support of code capabilities includes Gregory Bunting, Nathan Crane, David Day, Clark Dohrmann, Brian Ferri, Robert Flicek, Sean Hardesty, Payton Lindsay, Scott Miller, Lynn Munday, Brian Stevens, and Tim Walsh. The SIERRA/SD team also works closely with external collaborators in academia including Wilkins Aquino and Murthy Guddati.

Dozens of student interns have provided extensive support to the SIERRA/SD team in the fields of capability development and code testing. Additionally, the SIERRA/SD team is part of the larger Sierra Mechanics code team, receives extensive support from the

Sierra/DevOps and Sierra/Toolkit teams, and maintains close collaborations with the Sierra Solid Mechanics and Thermal Fluid teams.

The authors would like to thank John Fahnline of Penn State's Applied Research Lab for consulting on the bronze plate example.

References

[1] Shin, Y. S., 2004, "Ship Shock Modeling and Simulation for Far-Field Underwater Explosion," Comput. Struct., **82**(23), pp. 2211–2219.
[2] Gong, S., and Lam, K., 1999, "Transient Response of Floating Composite Ship Section Subjected to Underwater Shock," Compos. Struct., **46**(1), pp. 65–71.
[3] Molisani, L. R., Burdisso, R. A., and Tsihlas, D., 2003, "A Coupled Tire Structure/Acoustic Cavity Model," Int. J. Solids Struct., **40**(19), pp. 5125–5138.
[4] Diaz, C. G., Kindt, P., Middelberg, J., Vercammen, S., Thiry, C., Close, R., and Leyssens, J., 2016, "Dynamic Behaviour of a Rolling Tyre: Experimental and Numerical Analyses," J. Sound Vib., **364**, pp. 147–164.
[5] Ghangale, D., Colaço, A., Costa, P. A., and Arcos, R., 2019, "A Methodology Based on Structural Finite Element Method-Boundary Element Method and Acoustic Boundary Element Method Models in 2.5 D for the Prediction of Reradiated Noise in Railway-Induced Ground-Borne Vibration Problems," ASME J. Vib. Acoust., **141**(3), p. 031011.
[6] Schultz, R., and Walsh, T., 2016, *Rotating Machinery, Hybrid Test Methods, Vibro-Acoustics & Laser Vibrometry*, J. De Clerck and D. Epp, eds., Vol. 8, Springer, New York, pp. 231–242.
[7] Stasiunas, E. C., Schultz, R. A., and Ross, M. R., 2016, "Performing Direct-Field Acoustic Test Environments on a Sandia Flight System to Provide Data for Finite Element Simulation," *Rotating Machinery, Hybrid Test Methods, Vibro-Acoustics & Laser Vibrometry*, J. De Clerck and D. Epp, eds., Vol. 8, Springer, New York, pp. 267–279.
[8] Schultz, R., Ross, M., Stasiunas, E. C., and Walsh, T., 2016, "Finite Element Simulation of a Direct-Field Acoustic Test of a Flight System Using Acoustic Source Inversion," Tech. Rep., Sandia National Laboratories (SNL-NM), Albuquerque, NM.
[9] Yerrapragada, K., and Salehian, A., 2019, "Analytical Study of Coupling Effects for Vibrations of Cable-Harnessed Beam Structures," ASME J. Vib. Acoust., **141**(3), p. 031001.
[10] Huang, H., 1969, "Transient Interaction of Plane Acoustic Waves With a Spherical Elastic Shell," J. Acoust. Soc. Am., **45**(3), pp. 661–670.
[11] Fahnline, J. B., and Shepherd, M. R., 2017, "Transient Finite Element/Equivalent Sources Using Direct Coupling and Treating the Acoustic Coupling Matrix as Sparse," J. Acoust. Soc. Am., **142**(2), pp. 1011–1024.
[12] Atalla, N., and Sgard, F., 2015, *Finite Element and Boundary Methods in Structural Acoustics and Vibration*, CRC Press, Boca Raton, FL.
[13] Walsh, T., Jones, A., Bhardwaj, M., Dohrmann, C., Reese, G., and Wilson, R., 2013, "A Comparison of Transient Infinite Elements and Transient Kirchhoff Integral Methods for Far Field Acoustic Analysis," J. Comput. Acoust., **21**(2), p. 1350006.
[14] Bunting, G., Prakash, A., Walsh, T., and Dohrmann, C., 2018, "Parallel Ellipsoidal Perfectly Matched Layers for Acoustic Helmholtz Problems on Exterior Domains," J. Comput. Acoust., **26**(2), p. 1850015.
[15] Everstine, G., 1997, "Finite Element Formulations of Structural Acoustics Problems," Comput. Struct., **65**(3), pp. 307–321.
[16] Farhat, C., Van der Zee, K. G., and Geuzaine, P., 2006, "Provably Second-Order Time-Accurate Loosely-Coupled Solution Algorithms for Transient Nonlinear Computational Aeroelasticity," Comput. Methods Appl. Mech. Eng., **195**(17), pp. 1973–2001.
[17] Farhat, C., Lesoinne, M., and Le Tallec, P., 1998, "Load and Motion Transfer Algorithms for Fluid/Structure Interaction Problems With Non-Matching Discrete Interfaces: Momentum and Energy Conservation, Optimal Discretization and Application to Aeroelasticity," Comput. Methods Appl. Mech. Eng., **157**(1–2), pp. 95–114.
[18] Hambric, S. A., Sung, S. H., and Nefske, D. J., 2016, *Engineering Vibroacoustic Analysis: Methods and Applications*, John Wiley & Sons, New York.
[19] Beranek, L. L., and Piersol, A. G., 2006, *Noise and Vibration Control Engineering: Principles and Applications.*, John Wiley & Sons, Inc., Hoboken, NJ.
[20] Minami, S., Kawai, H., and Yoshimura, S., 2012, "Parallel Bdd-based Monolithic Approach for Acoustic Fluid–Structure Interaction," Comput. Mech., **50**(6), pp. 707–718.
[21] Ross, M. R., Felippa, C. A., Park, K., and Sprague, M. A., 2008, "Treatment of Acoustic Fluid–Structure Interaction by Localized Lagrange Multipliers: Formulation," Comput. Methods Appl. Mech. Eng., **197**(33), pp. 3057–3079.
[22] Ross, M. R., Sprague, M. A., Felippa, C. A., and Park, K., 2009, "Treatment of Acoustic Fluid–Structure Interaction by Localized Lagrange Multipliers and Comparison to Alternative Interface-Coupling Methods," Comput. Methods Appl. Mech. Eng., **198**(9), pp. 986–1005.
[23] Piperno, S., and Farhat, C., 2001, "Partitioned Procedures for the Transient Solution of Coupled Aeroelastic Problems–Part II: Energy Transfer Analysis and Three-Dimensional Applications," Comput. Methods Appl. Mech. Eng., **190**(24–25), pp. 3147–3170.
[24] Bunting, G., Crane, N. K., Day, D. M., Dohrmann, C. R., Ferri, B. A., Flicek, R. C., Hardesty, S., Lindsay, P., Miller, S. T., Munday, L., and Walsh, T., 2018, *Sierra Structural Dynamics-Users Notes 4.50*, Sandia National Laboratories, Albuquerque, NM.
[25] Bunting, G., Crane, N. K., Day, D. M., Dohrmann, C. R., Ferri, B. A., Flicek, R. C., Hardesty, S., Lindsay, P., Miller, S. T., Munday, L., and Walsh, T., 2018, *Sierra SD Theory Manual 4.50*, Sandia National Laboratories, Albuquerque, NM.
[26] Bunting, G., 2019, "Strong and Weak Scaling of the Sierra/SD Eigenvector Problem to a Billion Degrees of Freedom," SAND 2019–1217, Sandia National Lab. (SNL-NM), Albuquerque, NM.
[27] Aquino, W., Bunting, G., Miller, S. T., and Walsh, T. F., 2018, "A Gradient-Based Optimization Approach for the Detection of Partially Connected Surfaces Using Vibration Tests," Comput. Methods Appl. Mech. Eng., **345**, pp. 323–335.
[28] Moyer, T., Stergiou, J., Reese, G., Luton, J., and Abboud, N., 2016, "Navy Enhanced Sierra Mechanics (NESM): Toolbox for Predicting Navy Shock and Damage," Comput. Sci. Eng., **18**(6), pp. 10–18.
[29] Scavuzzo, R. J., and Pusey, H. C., 2000, *Naval Shock Analysis and Design*, Shock and Vibration Information Analysis Center, Booz-Allen and Hamilton, Incorporated, McLean, VA.
[30] Hughes, T. J., 2012, *The Finite Element Method: Linear Static and Dynamic Finite Element Analysis*, Courier Corporation, North Chelmsford, MA.
[31] Cook, R. D., Malkus, D. S., Plesha, M. E., and Witt, R. J., 2007, *Concepts and Applications of Finite Element Analysis*, John Wiley & Sons, New York.
[32] Felippa, C. A., Park, K., and Farhat, C., 2001, "Partitioned Analysis of Coupled Mechanical Systems," Comput. Methods Appl. Mech. Eng., **190**(24), pp. 3247–3270.